Research Article | Vol. 9, No. 1 | 1 Jan 2019 | OPTICAL MATERIALS EXPRESS 203
Optical Materials EXPRESS

Enhanced electro-optic performance of surface-treated nanowires: origin and mechanism of nanoscale current injection for reliable ultraviolet light-emitting diodes

DAVIDE PRIANTE,[1] MALLESWARARAO TANGI,[1] JUNG-WOOK MIN,[1] NASIR ALFARAJ,[1] JIAN WEI LIANG,[1] HAIDING SUN,[2] HALA H. ALHASHIM,[3] XIAOHANG LI,[2] ABDULRAHMAN M. ALBADRI,[4] AHMED Y. ALYAMANI,[4] TIEN KHEE NG,[1,5] AND BOON S. OOI[1,6]

[1]*King Abdullah University of Science and Technology (KAUST), Computer, Electrical, and Mathematical Sciences and Engineering Division, Photonics Laboratory, Thuwal 23955-6900, Saudi Arabia*
[2]*King Abdullah University of Science and Technology (KAUST), Computer, Electrical, and Mathematical Sciences and Engineering Division, Advanced Semiconductor Laboratory, Thuwal 23955-6900, Saudi Arabia*
[3]*Imam Abdulrahman bin Faisal University, Department of Physics, College of Science, Dammam 31441, Saudi Arabia*
[4]*National Center for Nanotechnology, King Abdulaziz City for Science and Technology (KACST), Riyadh, 11442-6086, Saudi Arabia*
[5]*tienkhee.ng@kaust.edu.sa*
[6]*boon.ooi@kaust.edu.sa*

Abstract: Self-assembled nanowires are posed to be viable alternatives to conventional planar structures, including the nitride epitaxy for optoelectronic, electronic and nano-energy applications. In many cases, current injection and extraction at the nanoscopic scale are essential for marked improvement at the macroscopic scale. In this investigation, we study the mechanism of nanoscale current injection and the origin of improvement of the flow of charged carriers at the group-III nitride semiconductor surface and metal-semiconductor interfaces. Conductive atomic force microscopy (c-AFM) and Kelvin probe force microscopy (KPFM) enable a rapid analysis of the electrical and morphological properties of single and ensemble nanostructures. The surface potential and current injection of AlGaN nanowire-based LEDs are spatially mapped before and after surface treatment with KOH solution. Treated-nanowires showed an improved current spreading and increased current injection by nearly 10×, reduced sub-turn-on voltage (as low as 5 V), and smaller series resistance. The reduced contact potential confirms the lower semiconductor/metal barrier, thus enabling larger carriers flow, and correlates with the 15% increase in injection efficiency in macroscopic LEDs. The improvement leads to the normalization of nanoscale electrical conducting properties of UV AlGaN-based nanowire-LEDs and lays the foundation for the realization of practical nanowire-based device applications.

1. Introduction

AlGaN-based UV nanowires light emitters have recently attracted attention due to their unique properties [1–3] that partly overcome the drawbacks of the more mature planar technology, such as spontaneous and piezoelectric polarization fields [4], high dislocation density [5], low p-doping efficiency [6], and light extraction efficiency [7]. Moreover, group-III nitride nanowires can be grown on CMOS-compatible and cost-effective substrate such as Si [8,9] and highly conductive metal substrates [10–14]. This allows better electrical and heat

#347612 https://doi.org/10.1364/OME.9.000203
Journal © 2019 Received 8 Oct 2018; revised 23 Nov 2018; accepted 2 Dec 2018; published 17 Dec 2018

Optical Materials EXPRESS

dissipation compared to the commercial AlN and sapphire substrates, and improves the overall device performance [15,16]. Therefore, they offer a promising future for applications in air purification, water disinfection, curing, phototherapy and the next generation of high resolution displays [17,18]. However, limitations in eventual electro-optical conversion devices remain elusive to the nanostructure community, in particular when practical electrical devices are developed. For instance, nanostructures suffer from the large density of surface states, caused by the high surface-to-volume ratio. The large depletion layer resulting from the Fermi level pinning decreases the density of free electrons toward the surface, increasing the non-radiative recombination and affecting the quantum efficiency of the devices [19]. Moreover, the small contact area and the self-assembled growth of nanowires, lead to non-uniformity and low carrier injection which subsequently lowers the injection efficiency.

Various approaches have been employed to overcome these issues, such as sulfur-based compounds [20–22] and large band-gap encapsulation layers [23]. Recently, the microscopic enhancement of luminescence of AlGaN-based nanowires LEDs by using KOH solution has been reported [24]. However, the nanoscale origin and the mechanism of such enhancement are yet to be clarified. In fact, the results do not elucidate how the uniform injection can be obtained in such inhomogeneous ensemble of nanowires. Without this information, the utilization of nanowires for electrical devices is therefore hampered.

Conductive atomic force microscopy (c-AFM) has been previously utilized to study the nanoscale behavior of single nanowires and to visualize the electrical inhomogeneity [25–29]. This powerful technique allows a systematic investigation of rapid electrical properties without directly fabricating the device, hence enabling an immediate feedback on the grown sample quality. Moreover, it is applicable to a large variety of nanostructures and nanomaterials with high aspect ratio for studying the optical and electrical interaction with the surface. Various single nanowire electrical measurements have been performed to analyze material properties such as specific contact resistivity [30], doping concentration [31] [2], and current-voltage characteristics [32]. However, most of these efforts are based on single nanowire which requires complicated and time-consuming fabrication processes, e.g. e-beam lithography, preventing an overall device evaluation in a relatively large scale. Thus, c-AFM highlights the advantage of electrical measurements not only in single nanowire but also a cluster of nanowires with overall picture of their electrical performance. Despite the insightful work using this technique to measure the single nanowire and to understand the failure mechanisms, a thorough study of the electrical performance relative to the poor injection current caused by the nanowires surface in large scale is still lacking, and requires significant investigation to advance this field and bridge the gap that currently exists with the thin film technology.

In this work we address the nanoscale current injection limitation of UV AlGaN nanowires by analyzing, for the first time, the origin that prevents the efficient carrier flow and distribution uniformity. c-AFM and KPFM techniques were used to measure the single nanowires, and to map the current and the contact potential difference distributions of ensembles of nanowires. KOH-treatment was utilized to remove oxides and flatten the contact surface hence enabling a larger number of nanowires to be electrically injected and contribute to the overall device characteristics enhancement. Higher injection current, lower sub-turn-on voltage and smaller series resistance were achieved for the KOH-treated samples, as well as more than 2 × lower contact potential, confirming the lower surface band-bending. Full device structures exhibited current density as high as 240 A/cm^2 compared to an average of 140 A/cm^2 for the as-grown samples. Moreover, 15% improvement in injection efficiency was achieved for the treated device samples. This study aims to give a deep understanding of the nanometer scale current injection mechanism among the self-assembled AlGaN-based nanowires, and provides insights towards enhanced current spreading, injection efficiency and overall UV device performance demonstration.

Optical Materials EXPRESS

2. Experimental section

The AlGaN-based nanowires were grown on a Ti-TaN metal bi-layer [33] deposited on a phosphorus-doped <100> silicon substrate (10^{-1} Ω·cm) under nitrogen-rich condition using a Veeco GEN 930 plasma-assisted molecular beam epitaxy (PA-MBE) system. The samples were thermally degassed in the MBE load-lock at 200 °C, in the buffer chamber at 600 °C and subsequently in the growth chamber at 900 °C. The growth was initiated with n-GaN seeds at a temperature of 485 °C for 10 min at a beam equivalent pressure (BEP) of 6.2×10^{-8} Torr and silicon effusion cell at 1165 °C. The plasma RF power and N_2 flow were kept at 350 W and 1.0 sccm, respectively for the whole growth process. To improve the crystal quality, a higher temperature (585 °C) n-GaN layer was grown, therefore achieving a total thickness of ~80 nm. An approximately 50 nm n-AlGaN cladding layer was grown at 640 °C and it was followed by 15 stacks of alternating $Al_yGa_{(1-y)}N$ quantum barrier (Al and Ga BEP of 1.5×10^{-8} and 3×10^{-8} Torr) and $Al_xGa_{(1-x)}N$ quantum disks (Al and Ga BEP of 0.75×10^{-8} and 4.5×10^{-8} Torr) (where $x < y$) grown at 640 °C and with thicknesses of 4 nm and 3 nm respectively. The p-AlGaN layer was then grown at 620 °C (Al and Ga BEP of 1.5×10^{-8} and 2×10^{-8} Torr), Mg temperature at 440 °C with a final thickness of ~50 nm. Finally, a p^+-AlGaN contact layer was grown with a thickness of ~20 nm (growth temperature of 580 °C and Mg temperature of 450 °C). After growth, two samples were treated in 10% KOH solution for 10 s and 40 s and a third sample was left untreated as a reference.

The morphology of the samples is evaluated using FEI Nova Nano 630 scanning electron microscope (SEM). The PL measurements are performed with a 266-nm pulsed laser (Teem Photonics SNU-20F-100; 10 mW average power, 0.7 kW peak power, 0.6 ns pulse width, 19 kHz repetition rate). Light is collected from the top using a 15 × objective lens (Thorlabs LMU-15X-UVB; focal length = 13 mm, numerical aperture = 0.32, anti-reflection (AR) coating for the 240-360 nm wavelength range). It then passes through a beam splitter (50:50, Thorlabs BSW19, AR coated for 250-450 nm) where it is distributed to the camera and to a spectrometer (QE Pro Ocean Optics, 185-1100 nm range). The 266-nm laser excitation is first filtered using a long-pass filter (Semrock LP02-266RU-25).

The surface morphology is measured using AFM (Agilent 5500 SPM with a scan range of 90 μm × 90 μm × 8 μm and a vertical noise of 0.016 nm) and c-AFM equipped with a conductive Pt/Ir-coated tip (BRUKER CONTV-PT, spring constant = 0.2 N/m). All tests are performed at room temperature. The KPFM measurements were takes using the same equipment. The contact potential difference (CPD) between the conductive tip and the AlGaN-based nanowires surface is measured by nullifying the tip-sample CPD, hence allowing almost zero surface band-bending caused by the tip. Both c-AFM and KPFM scans were taken at a speed of 0.8 inch/s and 512 points/line.

The UV AlGaN-based nanowires-LEDs were fabricated with the lithography technique. The KOH-treated sample was immersed in 10% KOH solution prior to deposit a 5 nm/5 nm Ni/Au ohmic contact. The evaporation is performed using the angle-deposition (45°) technique in an electron-beam evaporation chamber, therefore guaranteeing the metal to be deposited only on the top p-AlGaN contact. The samples are then annealed at 550 °C for 1 min (2 cycles) in ambient environment. The top Ni/Au (10 nm/200 nm) metal contact is then evaporated. The sample is subsequently loaded in the inductively coupled plasma reactive-ion etching (ICP-RIE) chamber to remove the back silicon dioxide and immediately loaded in the sputtering chamber for the deposition of Ti/Au (10 nm/150 nm) n-contact. The power – current – voltage (L-I-V) and the electroluminescence (EL) measurements are performed in a setup similar to the PL with a current source meter (Keithley 2116B) and a silicon photodetector (Newport 818-UV) connected to a Newport 1936-C power meter.

Optical Materials EXPRESS

3. Results and discussion

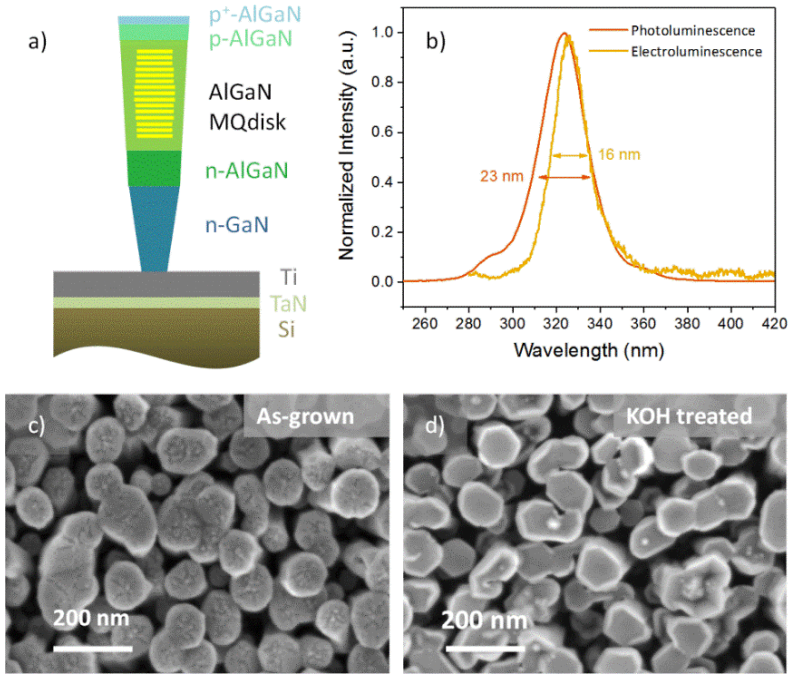

Fig. 1. (a) AlGaN multi quantum-disk (MQdisk) schematic nanowire device structure used in the experiment. (b) PL and EL spectrum. Top-view SEM images of: (c) as-grown AlGaN-based nanowires sample characterized by rough surface, and (d) AlGaN-based nanowires sample after 40 s KOH treatment showing smooth surface.

Figure 1(a) depicts the AlGaN nanowire structure grown on a metal bi-layer designed to improve the electrical injection and the heat dissipation. In this regard, we obtained lower junction temperature of samples grown on a metal-bilayer compared to silicon and AlGaN planar LEDs grown on sapphire [15]. The p-AlGaN/p^+-AlGaN layers were grown instead of the commonly used p-GaN, to reduce light absorption, therefore increasing light extraction. However, this constitutes a trade-off as the doping ionization efficiency reduces with increasing Al concentration, resulting in less free holes. In addition, we were able to achieve a hole concentration of 1.3×10^{19} cm^{-3} with large injection current [34].

The normalized PL and EL spectra of the as-grown AlGaN-based nanowires and fabricated device are shown in Fig. 1(b). The emission wavelengths match very well with the peak position centered at 325 nm. The full-width at half maximum (FWHM) is also measured to be 23 nm and 16 nm respectively. The slight greater FWHM in the PL measurement might be due to the high number of states that are excited by the high energy laser source as well as the large number of quantum disks that leads to inhomogeneous broadening of the spectrum and deviates from the theoretical $\Delta\lambda = 1.8\, kT\lambda^2/hc$ value, where $\Delta\lambda$, k, h and c are the FWHM, Boltzmann constant, Planck constant and speed of light. However, these values align well with previously reported AlGaN-based nanowires-LEDs [16] [35]. Furthermore, we recently reported PL and EL emission enhancement due to the increased radiative recombination as a consequence of the surface states passivation [24]. It is noted that the KOH-treated samples showed a longer carrier lifetime (slower non-radiative recombination) compared to as-grown samples at room temperature. This indicates a better radiative recombination (reduction of surface states). The small hump in the PL spectrum at ~290 nm is attributed to the higher Al composition barrier. Such peak, however, does not appear in the EL spectrum, confirming the high quantum confinement in the active region.

Optical Materials EXPRESS

Figures 1(c)-1(d) show the top view SEM images of the as-grown AlGaN-based nanowires and the 40 s KOH-treated nanowires. We can clearly notice that after treatment, the top p-AlGaN surface becomes smoother compared to the as-grown sample, signifying that KOH slightly etches the nanowires surface, despite the short treatment time. We have previously reported cross-sectional transmission electron microscopy images of KOH-treated samples where the surface of the AlGaN-based nanowires was flattened, hence confirming the treatment effects [24]. It is also noted that KOH is used to identify the material polarity. We recently demonstrated the pyramidal shape of InGaN/GaN nanowires after KOH etching that shows the N-polarity of the structure [36]. However, such process requires a 10-min KOH treatment that is much longer than the time employed in our experiment. Therefore, we can conclude that the short treating period used here only affects few nanometers of the AlGaN nanowires' surface.

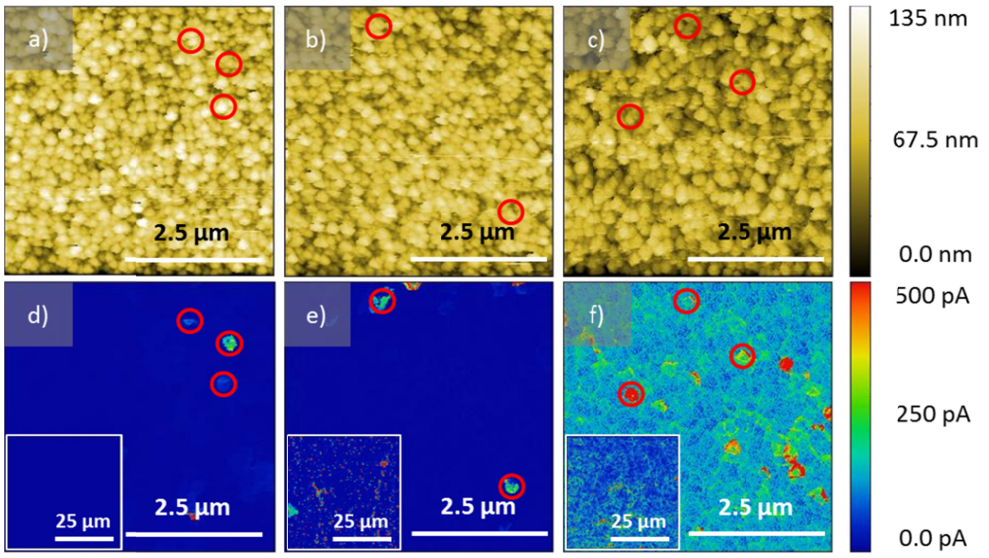

Fig. 2. (a-c) AFM 5 × 5 µm^2 scans of the as-grown, 10 s KOH and 40 s KOH samples respectively. (d-f) The corresponding current mapping showing higher current for the samples treated with KOH. The current range has been normalized to 500 pA for better comparison. Insets show the current mapping for an area of 50 × 50 µm^2.

The electrical characterization of AlGaN-based nanowires was performed using c-AFM. The average nanowire diameter is ~100 nm and being the c-AFM tip smaller, accurate single nanowire measurements can be performed. Figure 2 shows the AFM images (Figs. 2(a)-2(c)) and the current mapping (Figs. 2(d)-2(f)) of the as-grown, 10 s KOH-treated and 40 s KOH-treated AlGaN-based nanowires over a 5 × 5 µm^2 area. The corresponding current mappings are shown in Figs. 2(d)-2(f). Only few nanowires are injected in the as-grown sample, while clear improvement is noticed for the 40 s KOH sample with most of the nanowires showing high-current spots. The insets show 50 × 50 µm^2 areas current mapping. Despite a few spots that seem to pass larger current in the 10 s KOH sample, the 40 s KOH treated nanowires show a better current distribution, meaning that the slightly longer treatment time (40 s) helps in efficiently removing the surface oxide and to flatten the contact area, thus resulting in better metal (c-AFM tip)-semiconductor junction. This correlates well with our previous reported XPS results [24]. Before KOH treatment, the Ga 2p, Ga 3d, and Al 2p show peaks at 1117.7 eV, 19.9 eV and 74.4 eV (attributed to Ga-oxide and Al-oxide bonds), while after treatment the binding energy peaks shifted to lower values of 1117.0 eV, 19.3 eV and 73 eV (characteristics of Ga–N, Ga–N, and Al–N bonds). This has been attributed to the reduction of oxide bonds at the nanowire surfaces.

Optical Materials EXPRESS

We then measured the I-V curves of the three samples by sweeping the voltage from −6 to 10 V as shown in Fig. 3(a). Single nanowires were identified and tested, and the measurement was performed on different areas of the sample to have a better understanding of the inhomogeneity throughout the sample. One can notice that the as-grown sample shows the lowest current at the same voltage, while the values increase with KOH treatment time. A maximum current of ~1.4 nA was obtained for the 40 s KOH sample that corresponds to more than 1 order of magnitude higher than the as-grown sample. The 10 s KOH sample characteristics fall between the other two samples, meaning that the treatment time is not enough to obtain the highest device performance. All the three samples show a relatively large operation range, signifying that the non-uniformity among single nanowire plays an important role in the I-V curves [27]. Despite this, clear improvement was achieved by treating the nanowire samples with KOH. This can be explained by both surface oxide etching and flat surface (Fig. 1(b)) that allow better metal-semiconductor contact and current injection, as well as the removal of surface states at the nanowires sidewalls. It is worth mentioning that some electrical shorts exist in the sample, hence carrying most of the current injected [28]. However, the I-V characteristics of such nanowires have been removed for a more representative comparison.

The sub-turn-on voltages (non-abrupt V_{th}) are extracted by linearly fitting the high current (between 7.5 V and 10 V) segment of the curve (see blue dotted line in Fig. 3(a)). On average, lower V_{th} (~5 V) were obtained for the 40 s KOH samples, while similar values are shown for the other two samples. The V_{th} is slightly larger than the theoretical value of $V_{th} \approx V_D \approx E_g/e$, (where V_D, E_g and e are the diffusion voltage, energy bandgap and elementary charge, respectively) that is due to the common III-V semiconductor disadvantages such as bandgap discontinuities and contact resistance that cause additional voltage drop. Our results align well with previous report that showed an average turn-on voltage of 4.6 V for single AlGaN-based nanowire adopting a tunnel junction structure [27]. Therefore, we believe that by combining the tunnel junction and the KOH treatment, we would be able to reduce the operation voltage even further. Despite the deviation from the ideal I-V characteristics, lower series resistance was achieved for the 40 s KOH sample meaning that the contact resistance is reduced. The parallel resistance also plays a crucial role in nanowires due to the large surface-to-volume ratio. By decreasing the surface states with KOH, such resistances are reduced and improved I-V curves can be measured. The figure of merits extracted from the I-V curves are shown as histograms in Fig. 3(b).

Optical Materials EXPRESS

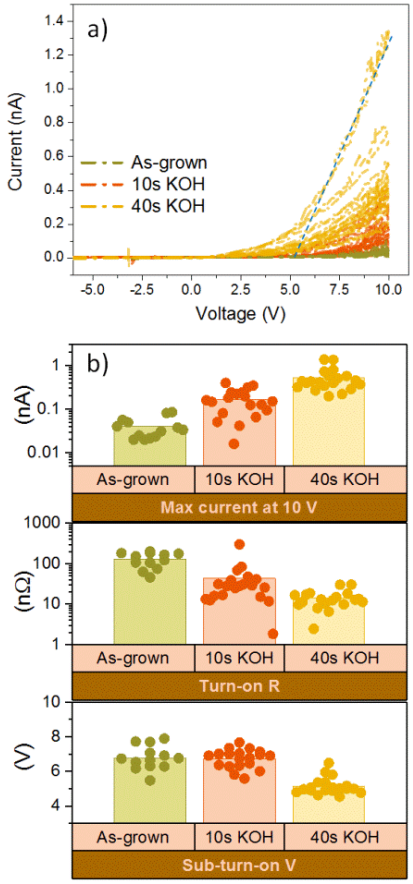

Fig. 3. (a) I-V curves of the three samples under test. (b) Histograms of the extracted figures of merit (maximum current, turn-on resistance, sub-turn-on voltage) of the three samples and the respective average values.

To study the structural and electrical properties of the AlGaN-based nanowires surface and interface, we utilized KPFM technique. KPFM allows the measurement of the surface potentials and offer indication on nanoscopic structural and chemical variations as well as on surface band bending, being the latter closely related to the potential profile when an electric field is applied. The contact potential difference measured by KPFM corresponds to the work function difference between the conductive tip and the sample. As reported by J. Bardeen, in a metal-semiconductor junction, such difference in work functions gives rise to a space charge region that in turn gives an electrostatic potential energy rise at the surface, i.e. the band bending [37]. Figure 4 shows the topography images and the corresponding CPD measurement on a 2×2 μm^2 area of the three samples. The red circles show the same spot for the specific sample. According to the scale bar on the right, a higher CPD is observed for the as-grown sample compared to the 10 s and 40 s KOH treated ones, which show lower CPD. This confirms the reduced potential barrier at the nanowires surface for the KOH-treated samples, compared to the as-grown sample where the presence of surface oxides clearly hinders the current flow (Fig. 3(a)). A line scan comparison over a 2 μm length is depicted in Fig. 4(g). It is noted that the spikes observed for the as-grown sample are attributed to the inhomogeneity within the as-grown single nanowires CPD. An overlap of the CPD mapping and the line scan is presented in Fig. 4(d) for the as-grown sample, showing the spikes caused by the inhomogeneous nanowires. However, these are not observed in the treated sample, meaning that a more uniform potential is obtained as a consequence of the KOH treatment

Optical Materials EXPRESS

that flatten the surface and remove the oxide. Figure 4(h) shows the average CPD values of the three samples. Our results show that both treated nanowire-samples have similar CPD values, which are far lower than that of the untreated sample. We hypothesize that the thickness of the residual native-oxide layer for both the treated samples are small but different, which is not clearly distinguishable by the CPD measurement in KPFM due to the noise level of this technique. However, this is clearly noticeable in the c-AFM measurements, which are essentially the tunnel currents through the combined Pt-Ir-tip/Ni-Au/native-oxide/p-AlGaN interfaces. In contrast, regardless of the similar CPD observed in KPFM measurements, a slight thickness variation of oxide layer would affect the tunneling current in the c-AFM measurements. The results emphasize that the 40s treated sample consists of the significantly reduced native-oxide layer, thereby exhibiting higher injection current as compared to the 10s treated and untreated samples.

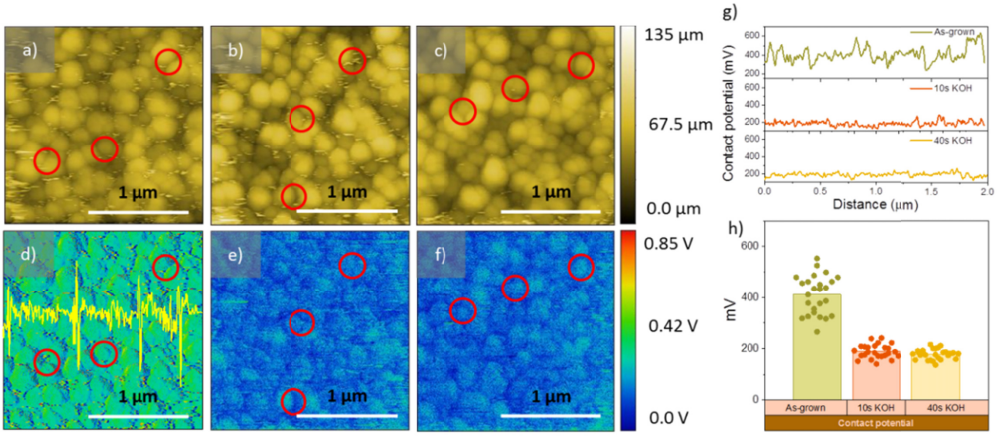

Fig. 4. (a-c) Comparison of AFM topography, and (d-f) CPD of the as-grown, 10 s and 40 s KOH samples respectively. The scan area is 2 × 2 µm^2. The yellow line in (d) is a line scan of the CPD for the as-grown sample. (g) Line scan of the CPD of the samples over a distance of 2 µm, and (h) histograms showing the average CPD values for ~25 different nanowires at various sample positions.

The full device electrical characterization results are shown in Fig. 5. Due to the better performance obtained from the 40 s KOH sample measured by c-AFM, we compared such device with the as-grown. Figures 5(a)-5(b) show the I-V curves and the extracted parameters of the two samples. Lower turn-on resistance and turn-on voltage are obtained for the 40 s KOH AlGaN-based nanowires device as well as higher current injection. In this regard, a current compliance of 600 mA (240 A/cm^2) was set in order to prevent the devices damage, as it can be seen in Fig. 5(a), meaning that higher values could be achieved. Such injection current is comparable with planar LEDs and it is considerably higher than other AlGaN-based nanowires devices [38,39]. This can be addressed to both the metal bi-layer substrate and the lower metal/semiconductor potential barrier (as shown in Fig. 4). Around 15 devices with an area of 0.5 × 0.5 mm^2 were tested on different parts of the wafer to have a wider statistical measurement. An average turn-on resistance of 7 Ω for the 40 s KOH sample was obtained, that is half of the average value of the as-grown sample (16 Ω), and much lower than previously AlGaN-based nanowires grown on metal substrate [34]. The turn-on voltage was reduced by 1 V showing an average value of 5.2 V (40 s KOH sample) and 6.2 V (as-grown) for the two samples, respectively. The slight turn-on voltage difference between the ensemble nanowires compared to the single nanowire (1 V vs. 1.6 V respectively) is likely due to the overall inhomogeneity of the measured group of nanowires. In fact, as reported in ref. 28, some nanowires are more resistive than others, hence increasing the overall device turn-on voltage. Despite this, the results align well with our previous work on KOH-treated self-

Optical Materials EXPRESS

ensemble AlGaN-based nanowires [24]. Moreover, the turn-on voltage is lower than other AlGaN studies, where values ranging from 6 V to 8 V have been reported [40] [9]. These results are even more remarkable considering that the common p-GaN top contact has been replaced by the more resistive p-AlGaN.

The relative EQE of an average sample was calculated by measuring the optical power and dividing it by the current injection, as depicted in Fig. 5(c). Higher values were obtained for the KOH-treated sample, confirming the better performances of the full device. The EQE increases with the current until 100 A/cm^2 after which it reaches a plateau. As mentioned above, the poor p-doping efficiency and the contact-barrier heights in GaN-based light-emitters highly hampers the carrier injection, reducing the overall EQE [41–43]. Therefore, to have a deeper understanding on the better current injection of the KOH-treated samples and to shed light on the electrical device performance, we studied the injection efficiency by employing the ABC model as follow [44]. We selected two devices (40 s KOH and as-grown) that showed an average current injection and EQE.

The injection efficiency can be calculated as a function of the EQE:

$$EQE = \eta_{int} \times \eta_{le} \times \eta_{inj}. \tag{1}$$

where η_{int}, η_{le} and η_{inj} are the internal quantum efficiency, light extraction efficiency and injection efficiency.

The η_{int} can be expressed as:

$$\eta_{int} = \frac{Bn^2}{An + Bn^2 + Cn^3}. \tag{2}$$

where A, B, C and n are the rate coefficients for the Shockley-Read-Hall, radiative and Auger recombination, and carrier concentration respectively. In steady state condition, the recombination rate con be considered equivalent to the carrier injection rate:

$$An + Bn^2 + Cn^3 = \frac{\eta_{inj} \times I}{qV_{QDs}}. \tag{3}$$

where the term on the left is the recombination rate at steady state and the term on the right is the carrier injection rate, q is the elementary charge and V_{QDs} is the volume of the nanowires quantum disks; we can then find a relation between the current density (J) and η_{inj}.

$$J \times \eta_{inj} = \left(An + Bn^2 + Cn^3\right) \times ql_{QDs}. \tag{4}$$

where l_{QDs} is the quantum disks thickness.

By inserting Eq. (2) into Eq. (1) and by considering Eq. (4), we can extract the carrier concentration as:

$$n = \sqrt{\frac{EQE \times J}{ql_{QDs} \times B \times \eta_{le}}}. \tag{5}$$

We can then obtain a cubic polynomial relation between J and $\sqrt{EQE \cdot J}$ by inserting Eq. (5) into Eq. (4):

$$J = \frac{A}{\eta_{inj}} \sqrt{\frac{ql_{QDs}}{B \times \eta_{le}}} \left(\sqrt{EQE \times J}\right) + \frac{1}{\eta_{inj} \times \eta_{le}} \left(\sqrt{EQE \times J}\right)^2 + \frac{C}{\eta_{inj}} \sqrt{\frac{1}{ql_{QDs} \times B^3 \times \eta_{le}^3}} \left(\sqrt{EQE \times J}\right)^3. \tag{6}$$

Optical Materials EXPRESS

Considering the J vs EQE curve in Fig. 5(c) we can then use the polynomial function to fit the J vs $\sqrt{EQE \cdot J}$ curve in Fig. 5(d), and extract the coefficients. It has been recently reported that the η_{le} of AlGaN-based nanowires can be enhanced for both TE and TM polarization by varying the tapering angle [3]. A maximum η_{le} for TE polarization was achieved with a tapering angle of 5.25 ° that perfectly represents our nanowires due to the same MBE growth conditions used. The $\eta_{inj} \cdot \eta_{le}$ can then be determined from the coefficient of the quadratic term. We considered a total η_{le} of 41.9% for our calculation and we obtained a 15% increment in η_{le} for the 40 s KOH sample compared to the as-grown. It is noted that other approaches have been adopted to calculate the η_{inj} and are based on EL, PL and IQE, and they all agreed that the low-current η_{inj} is equal to 1. This was confirmed by both simulation and experimental results. In fact, at low injection current the electron quasi Fermi level is low and the heating effects are not pronounced, therefore resulting in negligible carrier overflow. Despite the η_{inj} of the AlGaN-based nanowires remains low even after the KOH treatment (~1.3%), the improvement is evident, and it sets the foundation for improving the carrier injection characteristics of AlGaN-based nanowires devices.

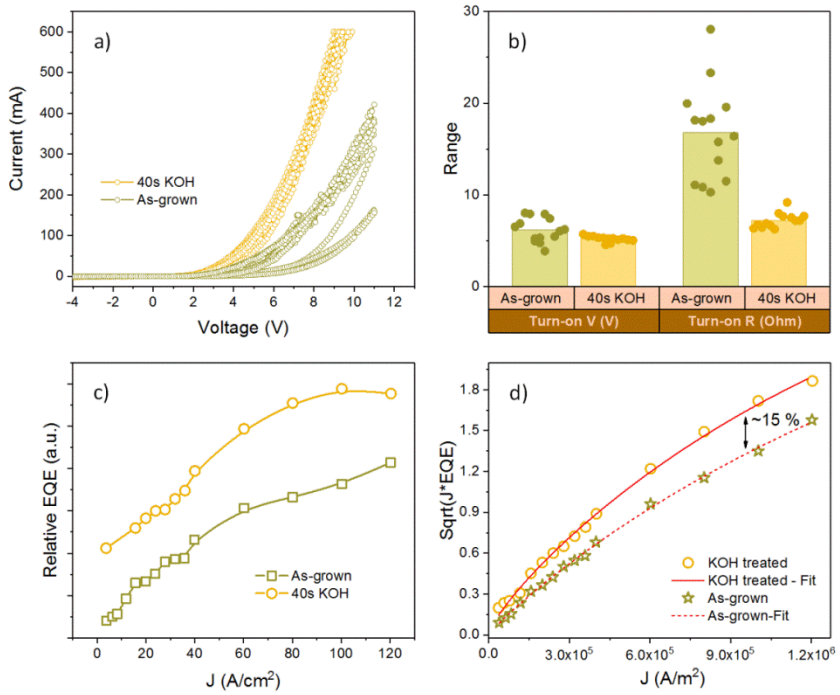

Fig. 5. (a) I-V curves of AlGaN-based nanowires-ensemble devices treated with 40 s KOH and that of the as-grown. (b) Comparative statistical analysis of the turn-on resistance and turn-on voltage extracted from the I-V curves. (c) Relative EQE comparison. (d) $\sqrt{J \cdot EQE}$' vs J plot and fitting lines showing an injection efficiency enhancement of 15% for the 40 s KOH-treated AlGaN-based nanowire-ensemble device.

4. Summary

Understanding the origin and mechanism of nanoscale current injection in nanostructures constitutes a critical effort towards the exploitation of a vast range of devices that rely on surface dynamics. We studied the AlGaN nanowires-based LEDs surface treatment by treating the samples with KOH solution to remove the surface oxide and reduce the semiconductor/metal potential barrier. By using c-AFM and KPFM, we provided a rapid statistical feedback on the nanoscale electrical and structural properties without the need of

Optical Materials EXPRESS

full devices fabrication. The single nanowire electrical characteristics clearly demonstrated the effectiveness and applicability of the facile and adaptable process, which can be applicable to a multitude of nanostructures. More specifically, KOH revealed a pristine and smooth semiconductor contact-layer with the end effect of lowering the contact potential barrier for the overall improvement in uniform metal-semiconductor interface and current injection. We achieved ~10 times higher current injection, reduced sub-turn-on voltage of 5 V and a lower average series resistance of 13 nΩ, compared to those of the un-treated as-grown samples (6.7 V and 170 nΩ). Finally, the characterization of fabricated LEDs correlates well with the observations, and an improvement of ~15% on the injection efficiency was measured. These results and techniques shed light on the central role of the nanoscale electrical measurement towards the realization of high-efficiency electro-optical nano- and macro-devices.

Funding

King Abdulaziz City for Science and Technology (KACST) (KACST TIC R2-FP-008); King Abdullah University of Science and Technology (KAUST) (BAS/1/1614-01-01, C/M-20000-12-001-77, BAS/1/1664-01-01, URF/1/3437-01-01) GCC Research Council Grant REP/1/3189-01-01; National Natural Science Foundation of China (Grant No. 61774065).

References

1. H. Sun, D. Priante, J. W. Min, R. C. Subedi, M. K. Shakfa, Z. Ren, K. H. Li, R. Lin, C. Zhao, T. K. Ng, J. H. Ryou, X. Zhang, B. S. Ooi, and X. Li, "Graded-Index Separate Confinement Heterostructure AlGaN Nanowires: Toward Ultraviolet Laser Diodes Implementation," ACS Photonics **5**(8), 3305–3314 (2018).
2. N. H. Tran, B. H. Le, S. Zhao, and Z. Mi, "On the mechanism of highly efficient p-type conduction of Mg-doped ultra-wide-bandgap AlN nanostructures," Appl. Phys. Lett. **110**(3), 032102 (2017).
3. R. Lin, S. V. Galan, H. Sun, Y. Hu, M. S. Alias, B. Janjua, T. K. Ng, B. S. Ooi, and X. Li, "Tapering-induced enhancement of light extraction efficiency of nanowire deep ultraviolet LED by theoretical simulations," Photon. Res. **6**(5), 457–462 (2018).
4. S. H. Park and S. L. Chuang, "Piezoelectric effects on electrical and optical properties of wurtzite GaN/AlGaN quantum well lasers," Appl. Phys. Lett. **72**(24), 3103–3105 (1998).
5. K. Ban, J. I. Yamamoto, K. Takeda, K. Ide, M. Iwaya, T. Takeuchi, S. Kamiyama, I. Akasaki, and H. Amano, "Internal quantum efficiency of whole-composition-range AlGaN multiquantum wells," Appl. Phys. Express **4**(5), 052101 (2011).
6. K. B. Nam, M. L. Nakarmi, J. Li, J. Y. Lin, and H. X. Jiang, "Mg acceptor level in AlN probed by deep ultraviolet photoluminescence," Appl. Phys. Lett. **83**(5), 878–880 (2003).
7. Han-Youl Ryu, Il-Gyun Choi, Hyo-Sik Choi, and Jong-In Shim, "Numerical investigation of light extraction efficiency in AlGaN deep ultraviolet light-emitting diodes," *2013 Conf. Lasers Electro-Optics Pacific Rim* (2013), pp. 1–2.
8. Z. Mi, "III-V compound semiconductor nanostructures on silicon: epitaxial growth, properties, and applications in light emitting diodes and lasers," J. Nanophotonics **3**(1), 031602 (2009).
9. B. Janjua, D. Priante, A. Prabaswara, L. Alanazi, C. Zhao, A. A. Alhamoud, M. S. Alias, A. M. Albadri, A. Y. Alyamani, T. K. Ng, and B. S. Ooi, "Ultraviolet-A LED Based on Quantum-Disks-In-AlGaN-Nanowires-Optimization and Device Reliability," IEEE Photonics J. **10**(2), 1 (2018).
10. A. T. M. Sarwar, S. D. Carnevale, F. Yang, T. F. Kent, J. J. Jamison, D. W. McComb, and R. C. Myers, "Semiconductor Nanowire Light-Emitting Diodes Grown on Metal: A Direction Toward Large-Scale Fabrication of Nanowire Devices," Small **11**(40), 5402–5408 (2015).
11. J.-W. Min, D. Priante, M. Tangi, G. Liu, C. H. Kang, A. Prabaswara, C. Zhao, L. Al-Maghrabi, Y. Alaskar, A. M. Albadri, A. Y. Alyamani, T. K. Ng, and B. S. Ooi, "Unleashing the potential of molecular beam epitaxy grown AlGaN-based ultraviolet-spectrum nanowires devices," J. Nanophotonics **12**(4), 1 (2018).
12. N. Alfaraj, S. Mitra, F. Wu, I. A. Ajia, B. Janjua, A. Prabaswara, R. A. Aljefri, H. Sun, T. Khee Ng, B. S. Ooi, I. S. Roqan, and X. Li, "Photoinduced entropy of InGaN/GaN p-i-n double-heterostructure nanowires," Appl. Phys. Lett. **110**(16), 1–6 (2017).
13. N. Alfaraj, M. M. Muhammed, K. H. Li, B. Janjua, R. A. Aljefri, H. Sun, T. K. Ng, B. S. Ooi, I. S. Roqan, and X. Li, "Thermodynamic photoinduced disorder in AlGaN nanowires," AIP Adv. **7**(11), 0–9 (2017).
14. C. Zhao, N. Alfaraj, R. Chandra Subedi, J. W. Liang, A. A. Alatawi, A. A. Alhamoud, M. Ebaid, M. S. Alias, T. K. Ng, and B. S. Ooi, "III-nitride nanowires on unconventional substrates: From materials to optoelectronic device applications," Prog. Quantum Electron. **61**(August), 1–31 (2018).
15. D. Priante, R. T. Elafandy, A. Prabaswara, B. Janjua, C. Zhao, M. Sharizal Alias, M. Tangi, Y. Alaskar, A. M. Albadri, A. Y. Alyamani, T. Khee Ng, and B. S. Ooi, "Diode junction temperature in ultraviolet AlGaN quantum-disks-in-nanowires," J. Appl. Phys. **124**(1), 015702 (2018).

Optical Materials EXPRESS

16. B. Janjua, H. Sun, C. Zhao, D. H. Anjum, D. Priante, A. A. Alhamoud, A. M. Albadri, A. Y. Alyamani, M. M. El-desouki, T. N. Khee, and B. S. Ooi, "Droop-free Al_x Ga_{1-x} N/A_{1y} Ga_{1-y} N quantum-disks- in-nanowires ultraviolet LED emitting at 337 nm on metal/silicon substrates," Opt. Express **25**(2), 1381–1390 (2017).
17. M. A. Khan, "AlGaN multiple quantum well based deep UV LEDs and their applications," Phys. Status Solidi Appl. Mater. Sci. **203**(7), 1764–1770 (2006).
18. T. D. Moustakas and R. Paiella, "Optoelectronic device physics and technology of nitride semiconductors from the UV to the terahertz," Rep. Prog. Phys. **80**(10), 106501 (2017).
19. R. Calarco, T. Stoica, O. Brandt, and L. Geelhaar, "Surface-induced effects in GaN nanowires," J. Mater. Res. **26**(17), 2157–2168 (2011).
20. H. P. T. Nguyen, M. Djavid, and Z. Mi, "Nonradiative recombination mechanism in phosphor-free GaN-based nanowire white light emitting diodes and the effect of ammonium sulfide surface passivation.," ECS Trans. **53**(2), Wide–Bandgap Semiconductor Materials and Devices 14), 93–100 (2013).
21. C. Zhao, T. K. Ng, A. Prabaswara, M. Conroy, S. Jahangir, T. Frost, J. O'Connell, J. D. Holmes, P. J. Parbrook, P. Bhattacharya, and B. S. Ooi, "An enhanced surface passivation effect in InGaN/GaN disk-in-nanowire light emitting diodes for mitigating Shockley-Read-Hall recombination," Nanoscale **7**(40), 16658–16665 (2015).
22. P. Varadhan, H. C. Fu, D. Priante, J. R. D. Retamal, C. Zhao, M. Ebaid, T. K. Ng, I. Ajia, S. Mitra, I. S. Roqan, B. S. Ooi, and J. H. He, "Surface Passivation of GaN Nanowires for Enhanced Photoelectrochemical Water-Splitting," Nano Lett. **17**(3), 1520–1528 (2017).
23. H. P. T. Nguyen, S. Zhang, A. T. Connie, M. G. Kibria, Q. Wang, I. Shih, and Z. Mi, "Breaking the carrier injection bottleneck of phosphor-free nanowire white light-emitting diodes," Nano Lett. **13**(11), 5437–5442 (2013).
24. H. Sun, M. K. Shakfa, M. M. Muhammed, B. Janjua, K. H. Li, R. Lin, T. K. Ng, I. S. Roqan, B. S. Ooi, and X. Li, "Surface-Passivated AlGaN Nanowires for Enhanced Luminescence of Ultraviolet Light Emitting Diodes," ACS Photonics **5**(3), 964–970 (2018).
25. S. G. Ihn, J. I. Song, T. W. Kim, D. S. Leem, T. Lee, S. G. Lee, E. K. Koh, and K. Song, "Morphology- and orientation-controlled gallium arsenide nanowires on silicon substrates," Nano Lett. **7**(1), 39–44 (2007).
26. F. Schuster, M. Hetzl, S. Weiszer, M. Wolfer, H. Kato, C. E. Nebel, J. A. Garrido, and M. Stutzmann, "Optoelectronic properties of p-diamond/n-GaN nanowire heterojunctions," J. Appl. Phys. **118**(15), 154303 (2015).
27. B. J. May, C. M. Selcu, A. T. M. G. Sarwar, and R. C. Myers, "Nanoscale current uniformity and injection efficiency of nanowire light emitting diodes," Appl. Phys. Lett. **112**(9), 093107 (2018).
28. B. J. May, M. R. Belz, A. Ahamed, A. T. M. G. Sarwar, C. M. Selcu, and R. C. Myers, "Nanoscale Electronic Conditioning for Improvement of Nanowire Light-Emitting-Diode Efficiency," ACS Nano **12**(4), 3551–3556 (2018).
29. M. Tangi, J.-W. Min, D. Priante, R. C. Subedi, D. H. Anjum, A. Prabaswara, N. Alfaraj, J. W. Liang, M. K. Shakfa, T. K. Ng, and B. S. Ooi, "Observation of piezotronic and piezo-phototronic effects in n-InGaN nanowires/Ti grown by molecular beam epitaxy," Nano Energy **54**(September), 264–271 (2018).
30. E. Stern, G. Cheng, M. P. Young, and M. A. Reed, "Specific contact resistivity of nanowire devices," Appl. Phys. Lett. **88**(5), 053106 (2006).
31. C. Y. Chang, G. C. Chi, W. M. Wang, L. I. C. Chen, K. H. Chen, F. Ren, and S. J. Pearton, "Electrical transport properties of single GaN and InN nanowires," J. Electron. Mater. **35**(4), 738–743 (2006).
32. G. Cheng, A. Kolmakov, Y. Zhang, M. Moskovits, R. Munden, M. A. Reed, G. Wang, D. Moses, and J. Zhang, "Current rectification in a single GaN nanowire with a well-defined p-n junction," Appl. Phys. Lett. **83**(8), 1578–1580 (2003).
33. D. Priante, B. Janjua, A. Prabaswara, R. C. Subedi, R. T. Elafandy, S. Lopatin, D. H. Anjum, C. Zhao, T. K. Ng, and B. S. Ooi, "Highly uniform ultraviolet-A quantum-confined AlGaN nanowire LEDs on metal/silicon with a TaN interlayer," Opt. Mater. Express **7**(12), 4214 (2017).
34. C. Zhao, M. Ebaid, H. Zhang, D. Priante, B. Janjua, D. Zhang, N. Wei, A. A. Alhamoud, M. K. Shakfa, T. K. Ng, and B. S. Ooi, "Quantified hole concentration in AlGaN nanowires for high-performance ultraviolet emitters," Nanoscale **10**(34), 15980–15988 (2018).
35. S. Zhao, S. M. Sadaf, S. Vanka, Y. Wang, R. Rashid, and Z. Mi, "Sub-milliwatt AlGaN nanowire tunnel junction deep ultraviolet light emitting diodes on silicon operating at 242 nm," Appl. Phys. Lett. **109**(20), 201106 (2016).
36. M. Tangi, P. Mishra, B. Janjua, A. Prabaswara, C. Zhao, D. Priante, J. W. Min, T. K. Ng, and B. S. Ooi, "Role of quantum-confined stark effect on bias dependent photoluminescence of N-polar GaN/InGaN multi-quantum disk amber light emitting diodes," J. Appl. Phys. **123**(10), 105702 (2018).
37. J. Bardeen, "Surface states and rectification at a metal semi-conductor contact," Phys. Rev. **71**(10), 717–727 (1947).
38. Q. Wang, A. T. Connie, H. P. T. Nguyen, M. G. Kibria, S. Zhao, S. Sharif, I. Shih, and Z. Mi, "Highly efficient, spectrally pure 340 nm ultraviolet emission from AlxGa□-xN nanowire based light emitting diodes," Nanotechnology **24**(34), 345201 (2013).
39. S. D. Carnevale, T. F. Kent, P. J. Phillips, M. J. Mills, S. Rajan, and R. C. Myers, "Polarization-induced pn diodes in wide-band-gap nanowires with ultraviolet electroluminescence," Nano Lett. **12**(2), 915–920 (2012).
40. K. H. Li, X. Liu, Q. Wang, S. Zhao, and Z. Mi, "Ultralow-threshold electrically injected AlGaN nanowire ultraviolet lasers on Si operating at low temperature," Nat. Nanotechnol. **10**(2), 140–144 (2015).
41. D. S. Lee, D. Byrnes, A. Parekh, S. Ting, and W. Quinn, "Carrier injection efficiency in nitride LEDs," J. Cryst.

Optical Materials EXPRESS

Growth **310**(23), 5158–5161 (2008).
42. L. Wang, J. Wang, H. Li, G. Xi, Y. Jiang, W. Zhao, Y. Han, and Y. Luo, "Study on injection efficiency in InGaN/GaN multiple quantum wells blue light emitting diodes," Appl. Phys. Express **1**(2), 021101 (2008).
43. I. V. Rozhansky and D. A. Zakheim, "Analysis of the causes of the decrease in the electroluminescence efficiency of AlGaInN light-emitting-diode heterostructures at high pumping density," Semiconductors **40**(7), 839–845 (2006).
44. J. Wang, T. Meisch, D. Heinz, R. Zeller, and F. Scholz, "Internal quantum efficiency and carrier injection efficiency of *c* -plane, $\{101\ \bar{1}\}$ and $\{112\ \bar{2}\}$ InGaN/GaN-based light-emitting diodes," Phys. Status Solidi **253**(1), 174–179 (2016).